Deep Learning Electronic Cleansing for Single- and Dual-Energy CT Colonography

Rie Tachibana, PhD[1]
Janne J. Näppi, PhD[1]
Junko Ota, PhD[2]
Nadja Kohlhase, MS[2]
Toru Hironaka, MS
Se Hyung Kim, MD
Daniele Regge, MD
Hiroyuki Yoshida, PhD

Electronic cleansing (EC) is used for computational removal of residual feces and fluid tagged with an orally administered contrast agent on CT colonographic images to improve the visibility of polyps during virtual endoscopic "fly-through" reading. A recent trend in CT colonography is to perform a low-dose CT scanning protocol with the patient having undergone reduced- or noncathartic bowel preparation. Although several EC schemes exist, they have been developed for use with cathartic bowel preparation and high-radiation-dose CT, and thus, at a low dose with noncathartic bowel preparation, they tend to generate cleansing artifacts that distract and mislead readers. Deep learning can be used for improvement of the image quality with EC at CT colonography. Deep learning EC can produce substantially fewer cleansing artifacts at dual-energy than at single-energy CT colonography, because the dual-energy information can be used to identify relevant material in the colon more precisely than is possible with the single x-ray attenuation value. Because the number of annotated training images is limited at CT colonography, transfer learning can be used for appropriate training of deep learning algorithms. The purposes of this article are to review the causes of cleansing artifacts that distract and mislead readers in conventional EC schemes, to describe the applications of deep learning and dual-energy CT colonography to EC of the colon, and to demonstrate the improvements in image quality with EC and deep learning at single-energy and dual-energy CT colonography with noncathartic bowel preparation.

Abbreviations: DCNN = deep convolutional neural network, EC = electronic cleansing, MFI = multimaterial feature image, 3D = three-dimensional

RadioGraphics 2018; 38:2034–2050

https://doi.org/10.1148/rg.2018170173

Content Code: IN

From the 3D Imaging Research Lab, Department of Radiology, Massachusetts General Hospital and Harvard Medical School, 25 New Chardon St, Suite 400C, Boston, MA 02114 (R.T., J.J.N., N.K., T.H., H.Y.); Department of Information Science and Technology, National Institute of Technology, Oshima College, Yamaguchi, Japan (R.T.); Department of Medical Physics and Engineering, Graduate School of Medicine, Osaka University, Suita, Osaka, Japan (J.O.); Department of Medical Physics, University of Applied Sciences Giessen, Giessen, Germany (N.K.); Department of Radiology, Seoul National University Hospital, Seoul, Republic of Korea (S.H.K.); Department of Surgical Sciences, University of Torino, Turin, Italy (D.R.); and Candiolo Cancer Institute, Fondazione del Piemonte per l'Oncologia–Istituto di Ricovero e Cura a Carattere Scientifico (FPO-IRCCS), Candiolo, Turin, Italy (D.R.). Presented as an education exhibit at the 2016 RSNA Annual Meeting. Received July 10, 2017; revision requested December 11 and received April 15, 2018; accepted April 26. For this journal-based SA-CME activity, the authors R.T., J.J.N., D.R., and H.Y. have provided disclosures (see end of article); all other authors, the editor, and the reviewers have disclosed no relevant relationships. **Address correspondence to** H.Y. (e-mail: *yoshida.hiro@mgh.harvard.edu*).

R.T. supported by the Japan Society for the Promotion of Science KAKENHI Grant-in-Aid for Young Scientists (A)(16H05913); J.J.N. and H.Y. supported by the National Institutes of Health, National Institute of Biomedical Imaging and Bioengineering, and National Cancer Institute (R21EB024025, R01CA166816, R01CA212382). The content is solely the responsibility of the authors and does not necessarily represent the official views of the National Institutes of Health.

[1]R.T. and J.J.N. contributed equally to this work.

[2]Current address: J.O.: Medical Informatics Section, Clinical Research Cluster, National Institute of Radiological Sciences, National Institutes for Quantum and Radiological Science and Technology, Chiba, Japan; N.K.: Institute of Medical Engineering University of Lübeck, Lübeck, Germany.

SA-CME LEARNING OBJECTIVES

After completing this journal-based SA-CME activity, participants will be able to:

- Describe the fundamentals of EC methods and the cleansing artifacts that the current EC methods generate.
- Discuss an effective application of deep learning to virtual bowel cleansing.
- Explain how the combined use of deep learning and dual-energy CT colonography can improve the image quality with EC.

See rsna.org/learning-center-rg.

TEACHING POINTS

- Electronic cleansing (EC) is an image postprocessing method for computational removal of contrast material–enhanced (tagged) fecal material from the colonic lumen on CT colonographic images.
- DCNNs have a built-in mechanism for automatic computation of optimal discriminating features directly from input images for precise classification of a target object on the images.
- With recent trends toward reducing bowel preparation requirements and radiation dose at CT colonography, conventional EC methods have been shown to produce cleansing artifacts that appear similar to or distort polyps on CT colonographic images, thereby distracting readers.
- Through its ability to allow differentiation of the chemical composition of materials, dual-energy CT circumvents the inherent problem of single-energy CT, which is that soft tissue is sometimes represented by CT values similar to those of unclearly tagged fecal material and partial-volume mixtures with air.
- Together, deep learning and dual-energy CT colonography are promising approaches for providing a next-generation EC scheme that is a substantial improvement on the quality of EC of the colon at CT colonography.

Introduction

Colorectal cancer is the third leading cause of cancer-related deaths in women and the second leading cause in men in the United States (1). Colorectal cancer screening facilitates not only early detection of cancers while they are still treatable but also prevention of cancers, because polyps can be detected and removed while they are still benign.

CT colonography, also known as virtual colonoscopy, is recommended by the U.S. Preventive Services Task Force and the American Cancer Society as an option for colorectal cancer screening (2,3). It provides a safe and accurate means of examining the complete region of the colon (4,5). Also, CT colonography does not necessarily require rigorous physical cathartic cleansing of the colon; thus it has the potential to increase patient compliance with colorectal cancer screening guidelines (6–9).

Patients typically prepare for a CT colonographic examination by orally ingesting an iodinated fecal-tagging contrast agent that enhances the fluid and stool that could obscure or resemble polyps on CT colonographic images (10). Electronic cleansing (EC) is an image postprocessing method for computational removal of contrast material–enhanced (tagged) fecal material from the colonic lumen on CT colonographic images. EC enables virtual endoscopic "fly-through" reading of a virtually reconstructed three-dimensional (3D) colonic surface for detection of polyps that otherwise would have been covered by fecal material (11). However, current EC methods have been developed mostly for single-energy CT colonography, where soft tissue can be confused with partial-volume tagging artifacts and unclearly tagged regions because of their similar CT values (12–15). Therefore, current EC methods can generate cleansing artifacts that distort normal anatomy and imitate polyps, thereby complicating the interpretation of virtually cleansed CT colonographic images. The current trend of using a very low-radiation-dose CT protocol and noncathartic bowel preparation tends to escalate this issue.

Attempts to perform EC with dual-energy CT colonography to reduce cleansing artifacts have been made (16,17). At two energy levels, two CT values of materials with a high effective atomic number deviate more from a linear relationship than do those of materials with a small effective atomic number (18,19). Therefore, dual-energy CT can be used to identify tagged and other materials and their partial-volume effects more precisely than can single-energy CT (20), and thus it has the potential to provide precise cleansing of the fecal materials in the colon.

Deep learning recently has become a popular method of choice in many applications (21). Especially in the interpretation of medical images, deep convolutional neural networks (DCNNs) have shown a remarkable ability to outperform conventional state-of-the-art classifiers in classification of abnormalities and disease patterns, and they are reaching interpretation levels comparable to those of human experts (22–25). Unlike conventional classification methods that use manually designed mathematical image features, DCNNs have a built-in mechanism for automatic computation of optimal discriminating features directly from input images for precise classification of a target object on the images (26). Therefore, DCNNs have the potential to provide precise electronic cleansing of the colon when they are applied to pixel and voxel classification of CT colonographic images and volumetric images.

In this article, we first review the causes of cleansing artifacts that distract and mislead readers of conventional CT colonographic images. We then describe how deep learning can be applied effectively to the EC of patients who undergo single- and dual-energy CT colonography. We also demonstrate the high cleansing quality of such a deep learning EC method at low-radiation-dose CT colonography for which patients have undergone reduced- or noncathartic bowel preparation.

Conventional EC: Artifacts and Pitfalls

Existing conventional EC methods originally were developed for CT colonographic examinations that involved rigorous cathartic bowel

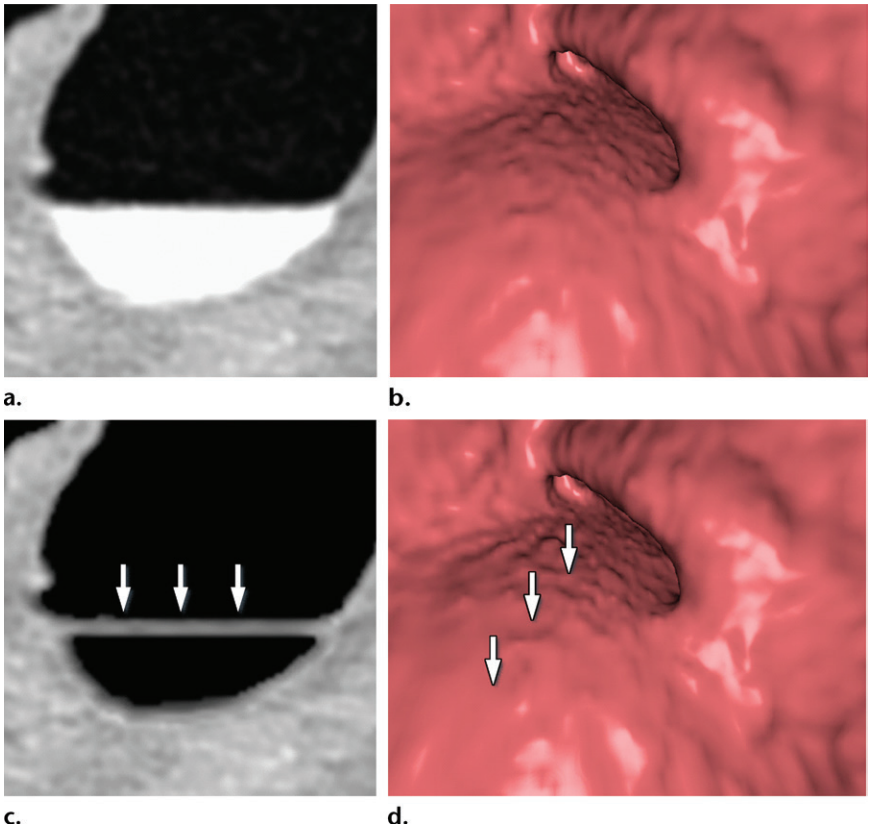

Figure 1. Type I cleansing artifact. **(a, b)** Original uncleansed axial CT colonographic image **(a)** and the corresponding virtual endoluminal view **(b)** show tagged fluid that obstructs the view of the bowel wall. **(c, d)** After cleansing with a conventional EC method, the corresponding axial image **(c)** and the virtual endoluminal view **(d)** show a Type I artifact of incomplete removal of the partial-volume boundary between air and tagged material (arrows on **c** and **d**).

preparation and a relatively high CT radiation dose (11). However, with recent trends toward reducing bowel preparation requirements and radiation dose at CT colonography, conventional EC methods have been shown to produce cleansing artifacts that appear similar to or distort polyps on CT colonographic images, thereby distracting readers (27).

Three types of cleansing artifacts commonly are observed. Type I (air-tagging boundary) artifacts are artificial residual soft-tissue layers that are caused by incomplete removal of partial-volume boundaries between air and tagged material (Fig 1). Type II (three-material boundary) artifacts are those that are incorrectly removed thin soft-tissue surfaces between air and tagged material (Fig 2), which occur when an EC method interprets the soft-tissue surface incorrectly as a Type I air-tagging boundary. Type III (three-material mixture) artifacts are partial-volume mixtures of air, soft tissue, and tagged material that are resolved unsatisfactorily with an EC method, thereby generating pseudopolyps or artificial diverticula (Fig 3). The three types of cleansing artifacts are caused largely by the inability of single-energy CT to allow differentiation among soft tissue, tagged fecal material, and their partial-volume mixtures with air.

Dual-Energy CT Colonography

Through its ability to allow differentiation of the chemical composition of materials, dual-energy CT circumvents the inherent problem of single-energy CT, which is that soft tissue is sometimes represented by CT values similar to those of unclearly tagged fecal material and partial-volume mixtures with air. The material decomposition can be performed by expressing the linear attenuation coefficient of a dual-energy CT image at energy E, μ^{E}, as a linear combination of the mass-attenuation coefficients of two basis materials at two energy levels (28).

$$\mu^{80\text{keV}} = m_1^{80\text{keV}} \cdot \rho_1 + m_2^{80\text{keV}} \cdot \rho_2$$

$$\mu^{140\text{keV}} = m_1^{140\text{keV}} \cdot \rho_1 + m_2^{140\text{keV}} \cdot \rho_2$$

where μ is the linear attenuation coefficient, $m_1^{80\text{keV}}$ and $m_1^{140\text{keV}}$ are the mass-attenuation coefficients of basis material 1 at 80 keV and 140 keV, respectively, and $m_2^{80\text{keV}}$ and $m_2^{140\text{keV}}$ are the mass-attenuation coefficients of basis material

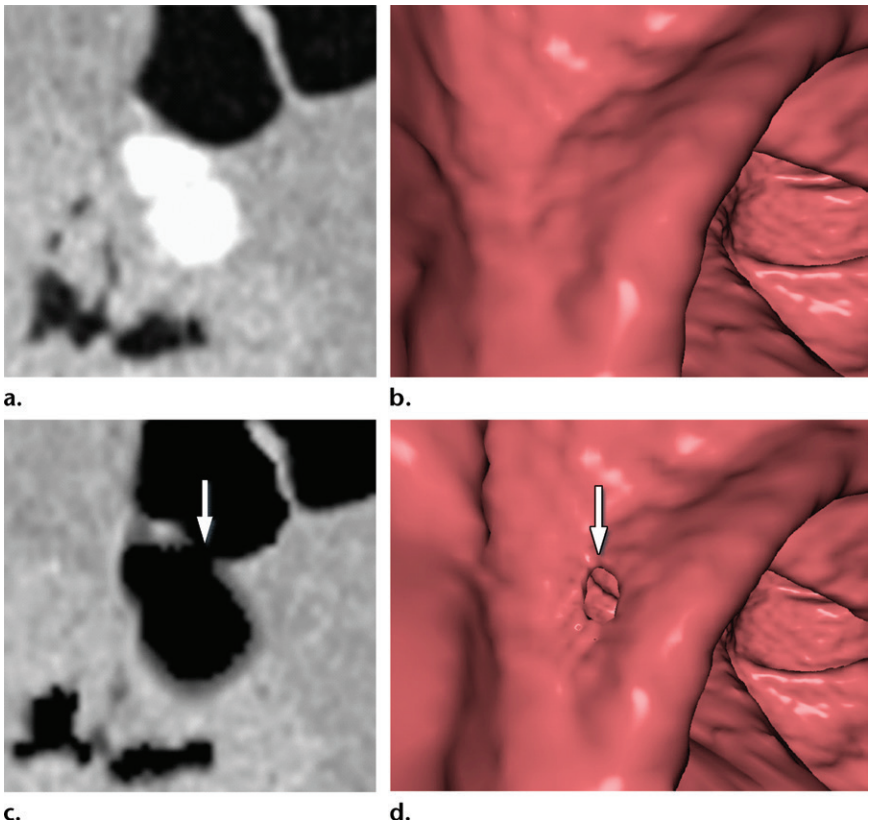

Figure 2. Type II cleansing artifact. **(a, b)** Original uncleansed axial CT colonographic image **(a)** shows tagged fecal material next to a thin fold, which appears complete on the corresponding virtual endoluminal view **(b)**. **(c, d)** After cleansing with a conventional EC method, the corresponding coronal image **(c)** and the virtual endoluminal view **(d)** show a Type II artifact of an incorrectly removed thin soft-tissue surface of the fold (arrow in **c** and **d**).

2 at 80 keV and 140 keV, respectively. The mass densities of the two basis materials, ρ_1 and ρ_2, can then be obtained by solving these two linear equations. At CT colonography, the basis materials of choice are typically water and iodine. By solving these equations for water and iodine, one obtains the material fractions of air, soft tissue, and iodine at each image voxel (29–31).

Dual-energy CT also can be used for calculation of virtual monochromatic images by reapplying the equations to the material decomposition images at a desired virtual monochromatic energy level. Virtual monochromatic images provide quantitatively more accurate attenuation measurements than do conventional single-energy CT colonographic images (18). With an appropriately chosen energy level, virtual monochromatic images also can be used to minimize the beam-hardening and pseudoenhancement artifacts that tend to appear around regions of highly attenuating tagged fecal material on single-energy CT colonographic images.

Deep Learning Electronic Cleansing

Most EC methods are based on the use of one or more image-based features to guide the cleansing of tagged fluid and feces on CT colonographic images. Traditionally, such features are designed manually on the basis of a mathematical model of cleansing. Our deep learning EC method derives such features automatically with the use of DCNNs. In the case of single-energy CT colonography, our method includes only one input volumetric image, the single-energy CT colonographic volumetric image, whereas in the case of dual-energy CT colonography, our method includes six input volumetric images: the two dual-energy CT colonographic volumetric images acquired with the dual-energy CT scanner, two material decomposition volumetric images, and two virtual monochromatic volumetric images. We use DCNNs to classify the image voxels of the input volumetric images into five key material and pseudomaterial classes needed for performing EC: air, soft tissue, tagged fecal material, the partial-volume boundary between air and tagged material, and the partial-volume boundary between soft tissue and tagged material (Fig 4). The volumetric image that indicates the spatial distribution of these material classes is called the multimaterial feature image (MFI) volume. We provide a

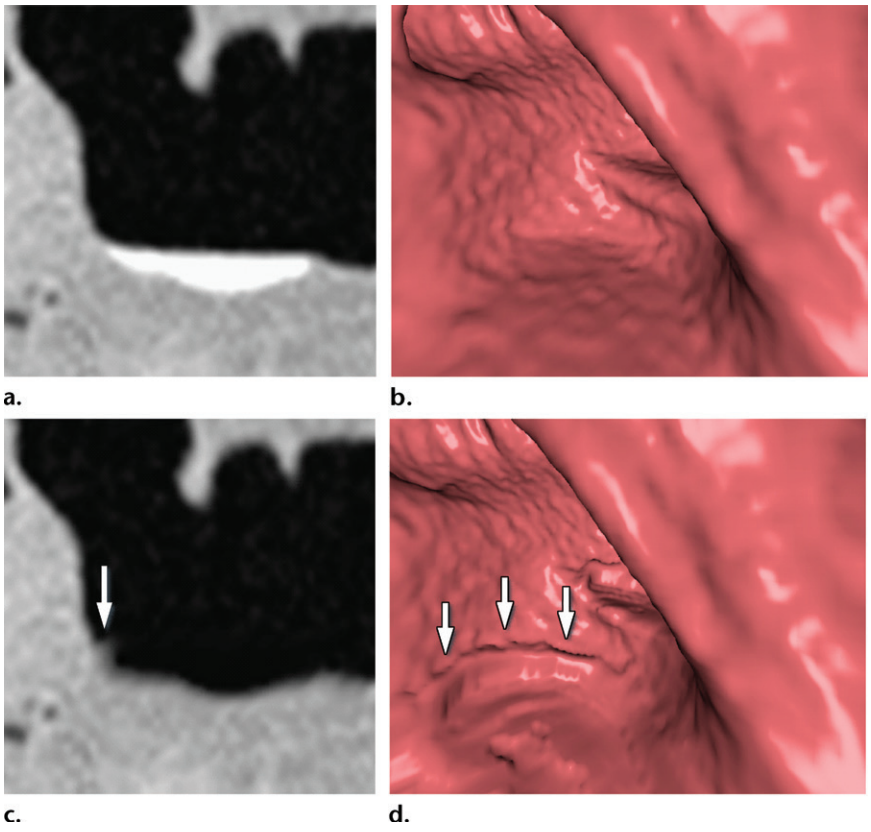

Figure 3. Type III cleansing artifact. **(a, b)** Original uncleansed sagittal CT colonographic image **(a)** shows tagged fecal material obstructing the bowel wall, as shown on the corresponding virtual endoluminal view **(b)**. **(c, d)** After cleansing with a conventional EC method, the corresponding sagittal image **(c)** and the virtual endoluminal view **(d)** show a Type III artifact, an unsatisfactorily resolved mixture of air, soft tissue, and tagged material (arrows in **c** and **d**).

general overview of our EC method, whereas the details of the training and evaluation of the DCNNs specific to the current study are provided in the "Deep Learning Single-Energy versus Dual-Energy EC Methods" section.

Transfer Learning of Deep Convolutional Networks

Before a DCNN is used, it must be trained. A DCNN has a large number of interconnected nodes that have been organized into several layers. The training of a DCNN involves adjustment of the connection weights and biases of the nodes so that it performs a desired computation (32). However, whereas a DCNN has a large number of such internal parameters to be adjusted, in medical imaging in general and in CT colonography in particular, the number of available appropriately annotated training cases is often limited.

In general, if the number or variety of training cases is limited, the DCNN is not able to classify new, unseen cases accurately. Transfer learning is an efficient paradigm for training highly complex classifiers when there are few domain-specific data (33–35). Transfer learning can be implemented by retraining a publicly available DCNN that has been pretrained with millions of general images by using domain-specific images. For application of such a pretrained DCNN to a new problem domain, only its highest layers must be retrained; this is because the bottom layers contain generic low-level image features such as edge-detection features that do not require retraining, whereas the highest layers are progressively more specific to the features of target classes of the original training data and thus must be retrained by using domain-specific images.

Voxel Classification with Deep Learning

CT colonography is a volumetric 3D imaging modality, whereas publicly available pretrained DCNNs suitable for transfer learning have been designed to classify two-dimensional images only. To incorporate the volumetric image information of CT datasets in our transfer learning EC method, we sampled multiple cut-plane region-of-interest images in symmetric 3D orientations at each voxel (Fig 5). Multiple

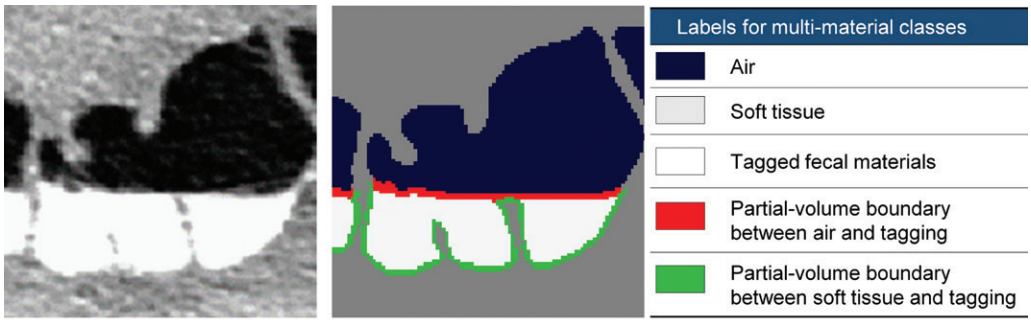

a. b.

Figure 4. Multimaterial classes used with our EC method. **(a)** Original CT colonographic image contains the three base material classes of lumen air, soft tissue, and tagged fecal material. **(b)** The corresponding reference-standard labels are manually prepared labels delineating the five multimaterial classes indicated in the table on the right.

DCNNs were then trained with transfer learning to classify these cut-plane images. The output of each DCNN is a probability vector that indicates the probabilities at which the center voxel of a region-of-interest image belongs to each of the five multimaterial classes. Each DCNN is specific to the type and 3D orientation at which the input region-of-interest image was sampled.

At each voxel, the outputs of the DCNNs are subjected to a metaclassifier (support vector machine [36,37]) for final prediction of the multimaterial class to which the voxel belongs. In this manner, the DCNNs form an ensemble classifier in which the output MFI volume represents the volumetric distribution of the five key material and pseudomaterial classes to perform the cleansing (38,39). Because DCNNs excel in multiclass classification tasks such as the classification of a voxel into multiple material classes (40), they enable us to calculate an optimal MFI volume (38,39).

Generation of the Final EC CT Colonographic Volumetric Image

By using the MFI volume, the final cleansed volumetric image is generated by converting the CT values at tagged voxels, which correspond to the MFI labels of tagged fecal material and the partial-volume boundary between air and tagged material, to the CT value of air (−1024 HU). However, a direct conversion could cause an unnaturally rapid transition of CT values at cleansed soft-tissue surfaces. Therefore, these surfaces are identified with the MFI volume label of the partial-volume boundary between soft tissue and tagged material, and they are reconstructed with a dedicated algorithm that assigns a predefined 3D intensity profile to the boundary for reconstruction of a realistic mucosal surface and performs 3D Gaussian smoothing for simulating the partial-volume effect between the soft-tissue surface and lumen air (12).

Improvements in EC with Deep Learning

Type I Artifacts

Figure 6 shows the cleansing of an inhomogeneous partial-volume boundary between air and tagged material. The deep learning single-energy EC scheme (third row) incorrectly retains some of the partial-volume boundary, thereby producing a Type I artifact. The automatically calculated MFI labels (Fig 6, *G*) indicate that the inhomogeneous portion of the boundary was labeled incorrectly as soft tissue, and thus it was retained on the virtually cleansed image. However, the deep learning dual-energy EC scheme (fourth row) identifies and thereby subtracts the entire partial-volume boundary correctly.

Type II Artifacts

Figure 7 shows the retention of a thin soft-tissue layer between air and tagged material. The deep learning single-energy EC scheme (third row) incorrectly removes part of the soft-tissue layer, thereby producing a Type II artifact. The automatically calculated MFI labels (Fig 7, *G*) indicate that the artifact was caused by incorrect interpretation of a portion of the layer as a partial-volume boundary between air and tagged material, which was then removed on the virtually cleansed image. However, the deep learning dual-energy EC scheme (fourth row) identifies and thereby retains the thin soft-tissue layer correctly.

Type III Artifacts

Figure 8 shows the cleansing of a multimaterial mixture of soft tissue, air, and tagged material. The deep learning single-energy EC scheme (third row) incorrectly identifies the junction of the air-tagging material boundary and colonic wall as soft tissue, thereby producing Type III artifacts that imitate the appearance of small polyps. The deep learning dual-energy EC scheme (fourth row)

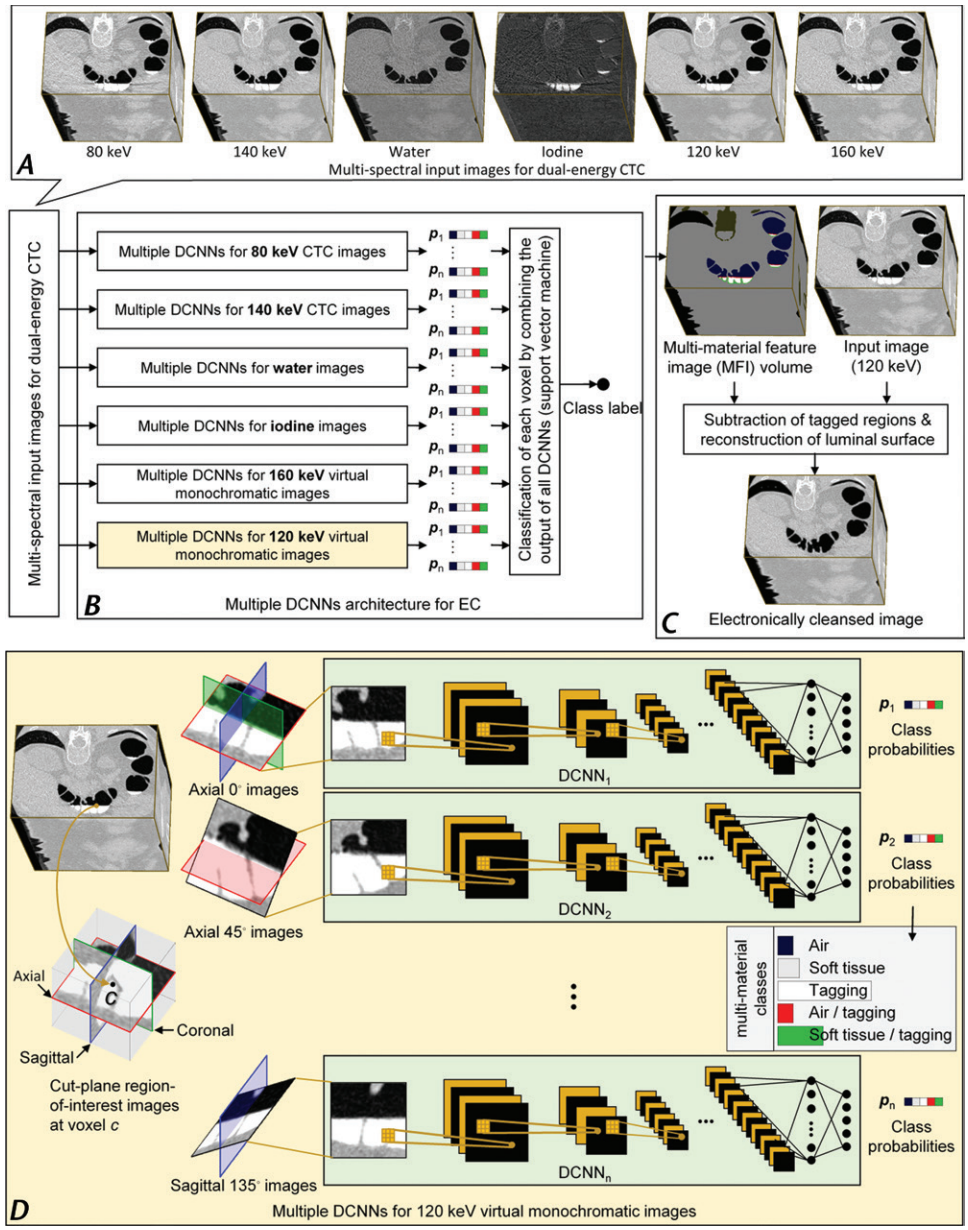

Figure 5. Schematic diagram of the deep learning EC method for dual-energy CT colonography (*CTC*). *(A–B)* An overview of the EC workflow shows that, *A,* six multispectral CT colonographic input volumetric images are reviewed by using, *B,* a DCNN ensemble classifier. The classifier consists of multiple DCNNs for reviewing each input volumetric image. With the use of output class probabilities of the individual DCNNs, a metaclassifier (support vector machine) determines the final multimaterial class labels for each voxel of an MFI volume. *C,* The virtually cleansed volumetric image is generated from a 120-keV CT colonographic volumetric image by converting its CT values that correspond to non–soft-tissue MFI volume labels to CT values of air, and by reconstructing cleansed soft-tissue surfaces within the MFI partial-volume boundary between soft tissue and tagged material. Each DCNN of the ensemble classifier in *B* has the same overall single-stream architecture. *D,* The regions of interest are represented by cut-plane images that are sampled at 0°, 45°, and 135° angles to the axial, coronal, and sagittal axes from the volumetric image. The use of multiple DCNNs allows calculation of class probabilities at each voxel from different input cut-plane region-of-interest images.

resolves the multimaterial mixture correctly, thereby producing correctly cleansed images.

Deep Learning Single-Energy versus Dual-Energy EC Methods

By using the principle of transfer learning, we acquired a Berkeley Vision and Learning Center Reference CaffeNet model (*http://caffe.berkeleyvision.org/*) that had been pretrained with 1.3 million images for 1000 natural object categories (41,42). We replaced the highest classification layer of the model with a randomly initialized classification layer for our five multimaterial classes. We then continued the training of the

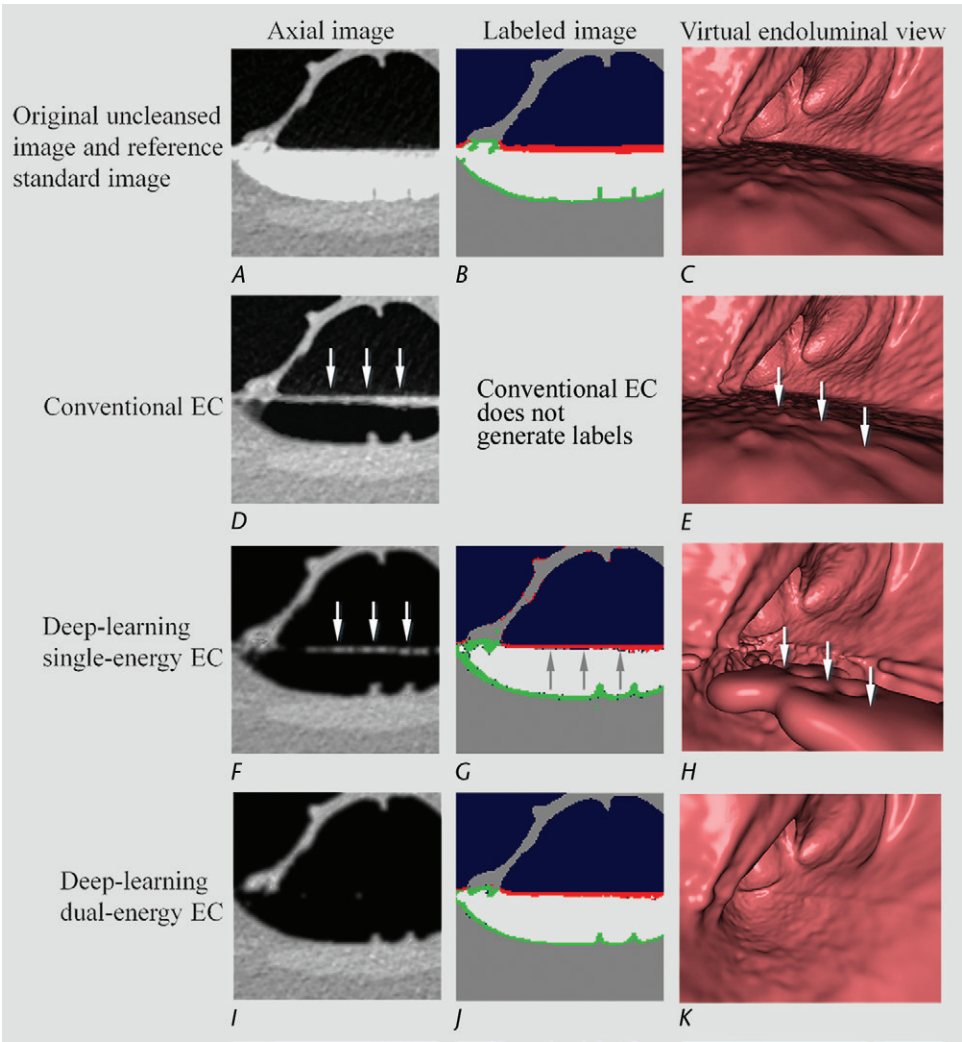

Figure 6. Electronic cleansing with Type I artifacts. *(A–C)* The first row shows, *A*, the original uncleansed axial CT colonographic image, *B*, the corresponding reference standard labels, and *C*, the uncleansed virtual endoluminal view. *(D, E)* The second row shows the outcome of a conventional EC method on, *D*, the axial CT colonographic image, and *E*, the virtual endoluminal view. White arrows on *D* and *E* indicate Type I artifacts. The corresponding space for the labeled image is kept blank, because the conventional EC method does not generate labels. (*F–H*) The third row shows the outcome of the deep learning single-energy EC on, *F*, the axial CT colonographic image, *G*, the corresponding automatically labeled image, and *H*, the corresponding virtual endoluminal view. The white arrows on *F* and *H* indicate Type I artifacts. The gray arrows on *G* indicate the portions of the partial-volume boundary between air and tagged material that were labeled incorrectly as soft tissue, and thus were causing the Type I artifacts. **(***I–K*) The fourth row shows the outcome of the application of the deep learning dual-energy EC, *I*, on the axial CT colonographic image, *J*, the corresponding automatically labeled image, and *K*, the corresponding virtual endoluminal view. The entire partial-volume boundary between air and tagged material was correctly identified and removed, and thus no Type I artifacts were generated.

DCNN for yielding labels for the MFI volumes on the basis of manually labeled reference standard MFI volumes (38,39). This enabled us to obtain rapidly an appropriately trained DCNN for each specific type of input image (eg, 120 keV virtual monochromatic images) (Fig 5).

Figure 9 shows a quantitative comparison of the accuracy of the deep learning single- and dual-energy EC schemes in cleansing of the colon regions that typically cause cleansing artifacts with a conventional EC method. The cleansing accuracy was quantified with the use of a two-fold cross-validation method with 384 volumes of interest extracted from the very low-radiation-dose CT colonographic images of 18 patients who underwent a noncathartic bowel preparation regimen. The CT colonographic images were acquired with the use of a dual-energy CT scanner (SOMATOM Definition Flash, Siemens Healthineers, Erlangen, Germany) and with the patient in supine and prone positions. The noncathartic bowel preparation regimen consisted of

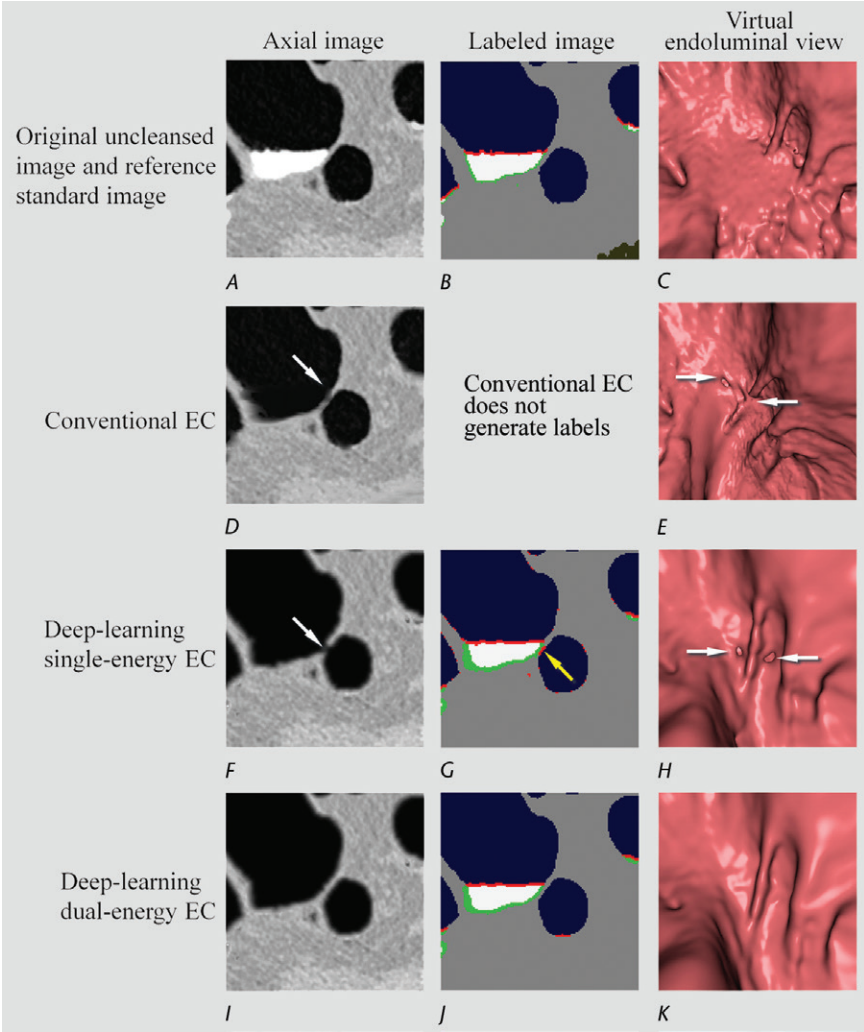

Figure 7. Electronic cleansing with Type II artifacts. (*A–C*) The first row shows, *A*, the original uncleansed axial CT colonographic image, *B*, the corresponding reference standard labeled image, and *C*, the corresponding uncleansed virtual endoluminal view. (*D, E*) The second row shows the outcome of a conventional EC method on, *D*, the axial image, and *E*, the corresponding virtual endoluminal view. The white arrows on *D* and *E* indicate Type II artifacts. The corresponding space for the labeled image is kept blank, because the conventional EC method does not generate labels. (F–H) The third row shows the outcome of the deep learning single-energy EC on, *F*, the axial CT colonographic image, *G*, the corresponding automatically labeled image, and *H*, the corresponding virtual endoluminal view. The white arrows on *F* and *H* indicate Type II artifacts. The yellow arrow on *G* indicates a portion of the soft tissue that was labeled incorrectly as a partial-volume boundary between air and tagged material and thus was the cause of the Type II artifacts. (*I–K*) The fourth row shows the outcome of the application of the deep learning dual-energy EC on, *I*, the axial CT colonographic image, *J*, the corresponding automatically labeled image, and *K*, the corresponding virtual endoluminal view. The entire thin layer between the air and tagged material is identified correctly as soft tissue, and thus no Type II artifacts were generated.

oral ingestion of 50 mL of the iodinated contrast agent amidotrizoate meglumine (Gastrografin; Bracco Diagnostics, Princeton, NJ) on the day before and 2 hours before the CT examinations. The CT section thickness was set to 0.6 mm, and the tube current was 25–36 mA at 140 kVp and 54–115 mA at 80 kVp for an average volume CT dose index of 0.95 mGy and an effective dose of 0.75 mSv. Single-energy CT colonographic images for these patients were obtained as virtual monochromatic images at 120 keV.

The accuracy of cleansing was measured by calculating the overlap ratio (OR):

$$\mathrm{OR}(V) = N(V) / R(V)$$

where $N(V)$ is the number of correctly assigned automatically calculated MFI volume labels (38,39), and $R(V)$ is the number of all voxels in the corresponding reference standard volumetric image. The reference standard volumetric images were prepared with 3D segmentation of the multimaterial classes (Fig 4) by three imaging scientists (R.T.,

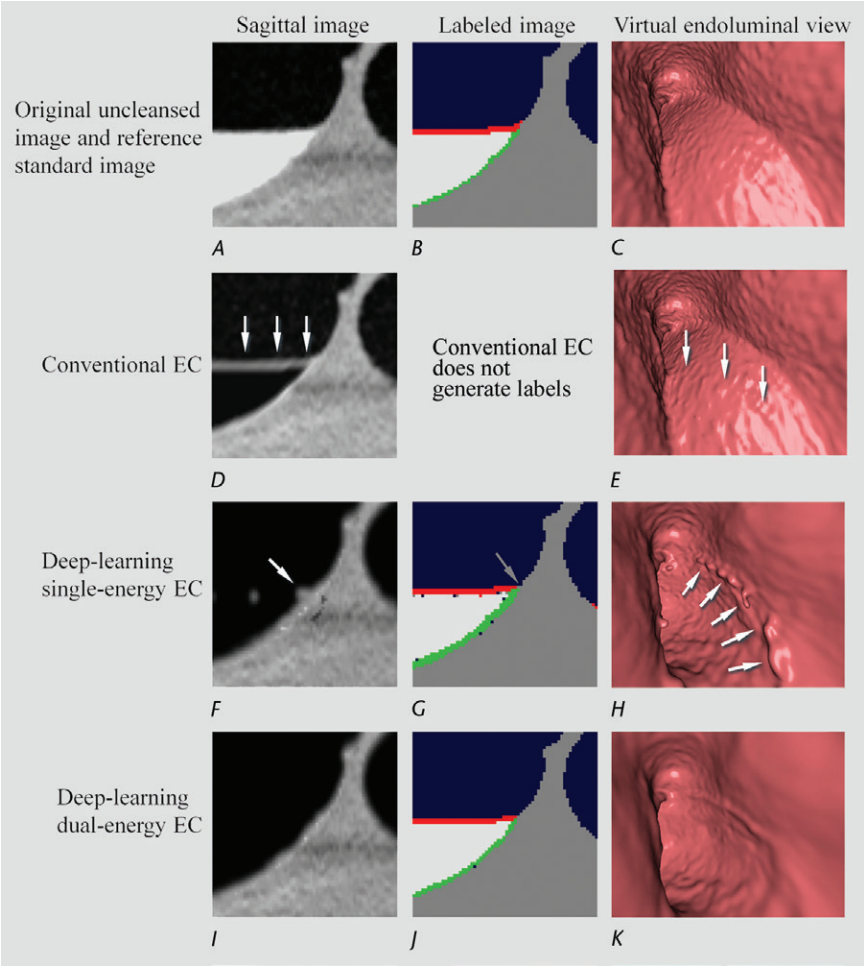

Figure 8. Electronic cleansing with Type III artifacts. (*A–C*) The first row shows, *A*, the original uncleansed sagittal CT colonographic image, *B*, the corresponding reference standard labeled image, and *C*, the corresponding uncleansed virtual endoluminal view. (*D, E*) The second row shows the outcome of conventional EC on, *D*, the sagittal CT colonographic image and *E*, the virtual endoluminal view. The white arrows on *D* and *E* indicate Type I artifacts. The corresponding space for the labeled image is kept blank, because the conventional EC method does not generate labels. (*F–H*) The third row shows the outcome of the deep learning single-energy EC on, *F*, the sagittal CT colonographic image, *G*, the automatically labeled image, and *H*, the virtual endoluminal view. The gray arrow on *G* indicates that the junction of air, tagged material, and colonic wall is identified incorrectly as soft tissue, thereby generating the Type III artifacts indicated by white arrows on *F* and *H*. (*I–K*) The fourth row shows the outcome of the application of the deep learning dual-energy EC scheme on, *I*, the sagittal CT colonographic image, *J*, the corresponding automatically labeled image, and *K*, the corresponding virtual endoluminal view. No type III artifacts were generated with this scheme.

J.O., and N.K., with 4, 2, and 1 years of experience in CT colonography) who used ITK-SNAP (*www.itksnap.org* [43]), which is open-source software for image segmentation and registration. The box plot of the accuracy (overlap ratios) in Figure 9 indicates that the use of dual-energy CT colonographic images yields consistently higher accuracy in cleansing of the colon than does the use of single-energy CT colonographic images for all three types of cleansing artifacts.

Lumen Coverage

Figure 10 shows the effect of cleansing on the virtual 3D reconstruction and lumen coverage of the colon. The uncleansed colon (Fig 10a) has pink regions that represent tagged fecal material covering parts of the colon surface. A commercially available (conventional) single-energy EC method (Fig 10b) retains some of the residual fluid and/or feces and thus fails to cover the complete region of the colonic lumen (a section of the descending colon is missing), whereas the deep learning dual-energy EC scheme (Fig 10c) removes all of the residual fluid and feces correctly, thereby facilitating complete fly-through visualization of the region of the colonic surface without the presence of obstructing fecal material.

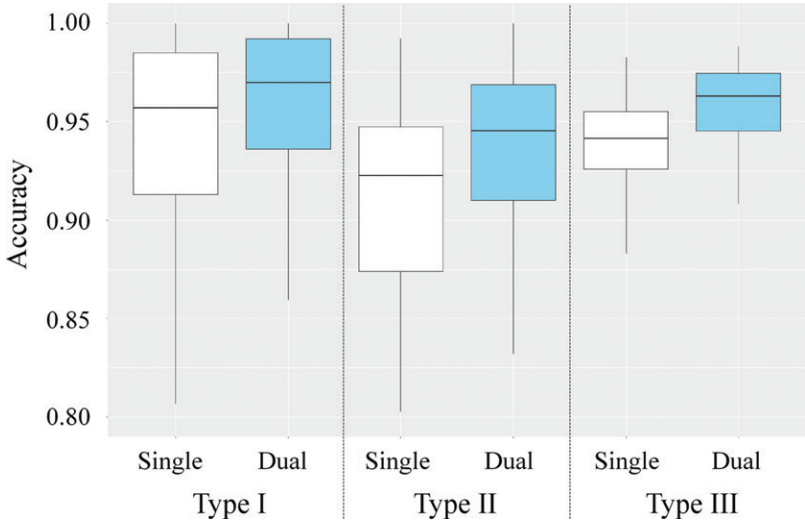

Figure 9. Box plot shows a quantitative comparison of the accuracy of the MFI volume labels automatically calculated by deep learning single- and dual-energy EC schemes for cleansing of regions affected by the three types of artifacts and that of a conventional EC method. The metric for accuracy was the overlap ratio between the automatically calculated MFI volume labels and the manually labeled reference-standard volume labels. The box plot was calculated from 384 volumes of interest sampled from 18 patients, where each of the three types of artifacts was represented by 128 volumes of interest.

Quality of Images Virtually Cleansed with Conventional versus Deep Learning EC Schemes

To date and to our knowledge, there have not been studies performed to compare deep learning EC schemes with conventional commercially available EC methods. However, we previously performed experiments (38) in which we compared deep learning EC schemes with simulated conventional EC methods in combination with single-energy CT colonography and multienergy CT colonography. When the cleansing performance was quantified with manually labeled volumetric images, the use of deep learning EC with multienergy features yielded the highest performance, with a statistically significant improvement in the overlap metric (increasing from 0.89 to 0.94) in comparison with a conventional machine-learning EC with multienergy CT colonography ($P < .001$). Without the use of multienergy features, the performance of deep learning EC (0.87) was significantly lower than that with multienergy CT colonography ($P < .001$).

In another study (44) in which noncathartic bowel preparation was used with very low-radiation-dose dual-energy CT colonography, the overlap metric used to quantify the cleansing performance was significantly higher with deep learning EC than that with conventional EC methods based on *k*-nearest neighbor or random forest classifiers.

Figures 11–13 show how cleansing with deep learning single-energy EC and dual-energy EC schemes produces fewer cleansing artifacts than does commercially available conventional EC software. The use of the deep learning dual-energy EC scheme tends to produce the least amount of cleansing artifacts. In these examples, all three EC schemes used the same uncleansed virtual monochromatic volumetric image as input.

Figure 11 shows a 10-mm polyp submerged in tagged fluid. The conventional EC method incorrectly retains the partial-volume boundary between air and fluid, thereby preventing the polyp from being seen. The deep learning single-energy EC scheme removes the partial-volume boundary and makes the polyp visible; however, some Type III artifacts that distort the endoluminal view remain. The deep learning dual-energy EC scheme correctly removes the tagged fluid from the images without generating any artifacts.

Figure 12 shows another 10-mm polyp submerged in fluid adjacent to the colonic wall. This is a challenging case, because the polyp could be interpreted incorrectly as a partial-volume three-material junction of air, soft tissue, and tagged fecal material. The conventional EC method resolves the three-material mixture incorrectly, thereby producing a Type III artifact and distorting the shape of the polyp. The deep learning single-energy EC method preserves the shape of the polyp more faithfully than does the conventional EC method, although some Type III artifacts remain. The deep learning dual-energy EC scheme removes the tagged fluid correctly from the images without generating any artifacts.

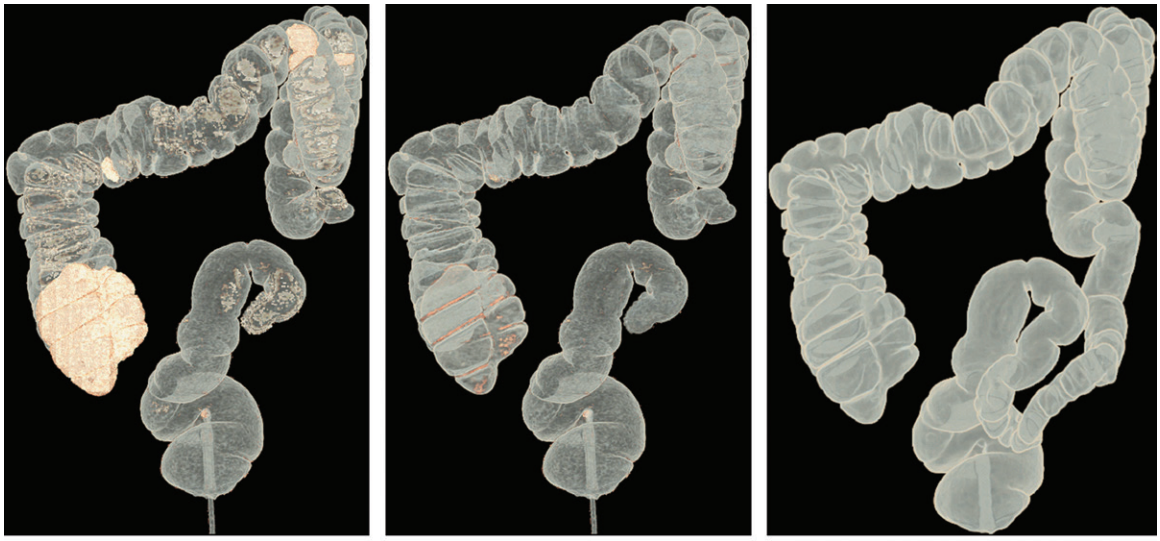

a. b. c.

Figure 10. Virtual 3D reconstructions of a colon from virtual monochromatic CT colonographic images before and after virtual cleansing. **(a)** The uncleansed volume has residual materials (pink regions in **a**) distributed throughout the colon, and part of the descending colon is completely missing from the reconstruction due to a major obstruction of the lumen by the residual materials. **(b)** The corresponding volume that was virtually cleansed with a conventional EC method shows that some of the residual materials are still retained in the colon and that the reconstruction of the descending colon is still incomplete. **(c)** The corresponding volume that was virtually cleansed by our deep learning dual-energy EC scheme shows that all of the residual materials have been removed, and this also has enabled complete reconstruction of the descending colon for complete fly-through visualization.

Figure 13 shows a 6-mm polyp submerged in semisolid feces. This is a challenging case, because part of the polyp could be interpreted incorrectly as a part of the partial-volume boundary between air and tagged material. Cleansing with the conventional EC method removes part of the polyp while retaining some tagged residual feces, which makes the polyp difficult to see in the endoluminal view. Cleansing with the deep learning single-energy EC scheme is more accurate, but it also reduces the apparent size of the polyp. Cleansing with the deep learning dual-energy EC scheme preserves the size of the polyp without producing cleansing artifacts.

Limitations of Deep Learning EC

One of the limitations of current deep learning EC schemes is that supervised training of DCNNs requires a large number of annotated samples. The samples should be annotated accurately by multiple experts, and multiple pathologic diagnoses should be represented. Errors or disagreements in the annotations can reduce the performance of trained DCNNs. Furthermore, as new samples with higher image quality than previous samples become available, the annotated cases should be updated accordingly. This is a time-consuming and costly process.

Although one can apply transfer learning to make use of pretrained classifiers, the dimensions of the input and output of the pretrained classifier must be compatible with those of the current case. Currently available pretrained classifiers have been trained with relatively low-resolution two-dimensional 8-bit color photographs with a fixed image size. Optimal transfer learning of CT images requires pretraining with high-resolution 3D medical datasets with 16-bit depth.

Deep learning EC does not allow interpretation of situations that it has not been trained to interpret. For example, if the method has not been trained to identify metallic, motion, and beam-hardening artifacts or image noise, these artifacts are interpreted according to the object categories that were used for training the network. Therefore, an effective deep learning EC should be trained not only with tagged fecal material but also with a wide variety of examples of normal anatomy. Ideally, those examples also should be annotated into distinct categories to help in understanding the decisions made with deep learning (45).

Currently available deep learning EC methods do not allow reliable differentiation between partial-volume effects of fecal material and thin soft-tissue layers that appear "sandwiched" between tagged regions. One of the problems is that such soft-tissue layers tend to be distorted by pseudoenhancement artifacts that cause soft-tissue layers to imitate partial-volume effects of fecal materials (46), and the number of training samples that represent such circumstances is relatively low. A more comprehensive training dataset would be needed for such artifacts to be addressed.

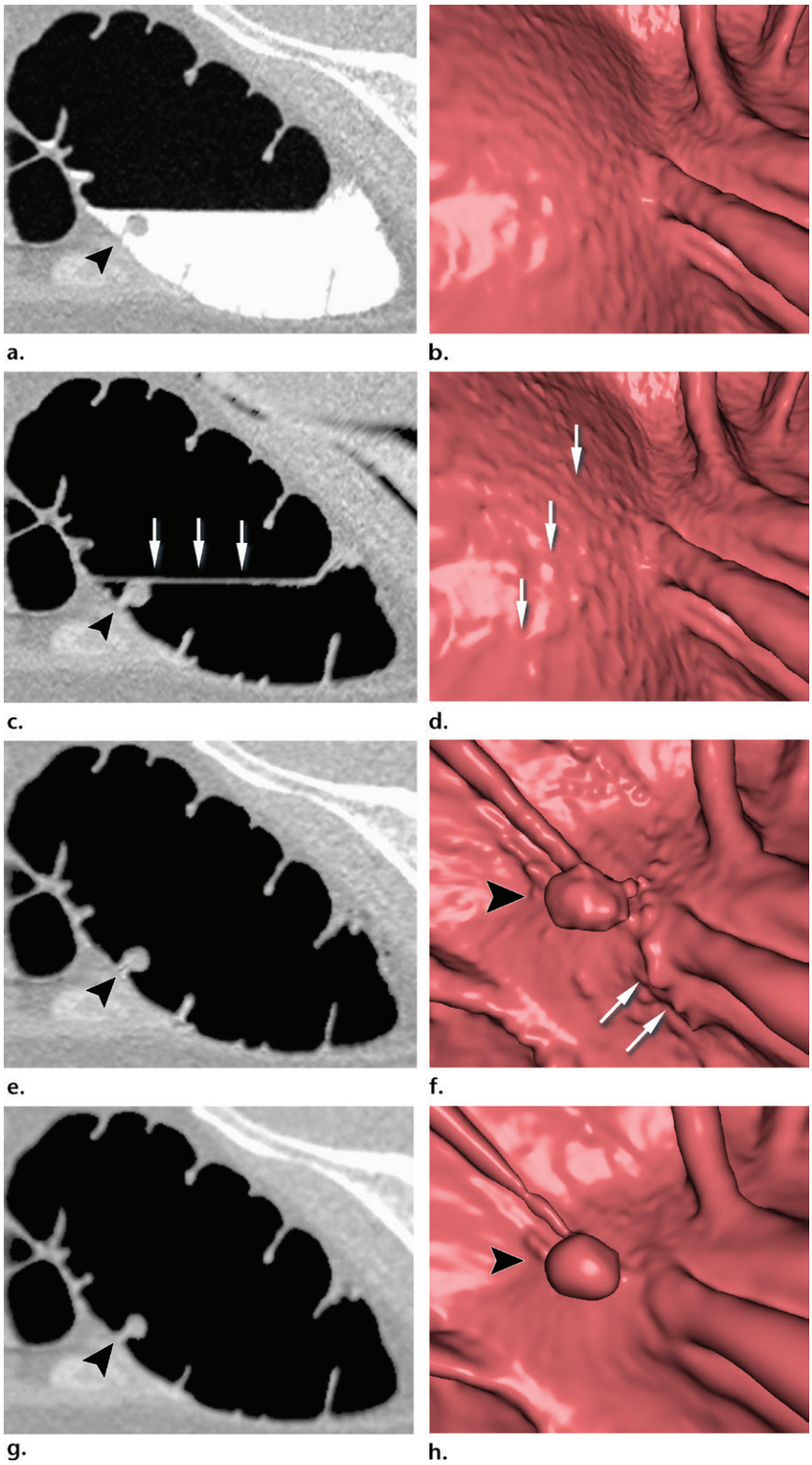

Figure 11. Electronic cleansing of tagged fluid with a submerged 10-mm polyp (arrowhead in **a**, **c**, **e**–**h**). **(a, b)** Uncleansed sagittal CT colonographic image **(a)** and the corresponding uncleansed virtual endoluminal view **(b)** show how the fluid obstructs the view of the colonic wall, including the polyp. **(c, d)** After cleansing with a conventional EC method, the corresponding sagittal image **(c)** and virtual endoluminal image **(d)** show a Type I artifact (white arrows) that still prevents the submerged polyp and the colonic wall from being seen. **(e, f)** After cleansing with our deep learning single-energy EC scheme, the sagittal image **(e)** and virtual endoluminal view **(f)** show that the polyp is visible; however, the virtual endoluminal view is distorted by Type III artifacts (white arrows in **f**). **(g, h)** After cleansing with our deep learning dual-energy EC scheme, the sagittal image **(g)** and virtual endoluminal image **(h)** show that the polyp is visible and that there are no image artifacts.

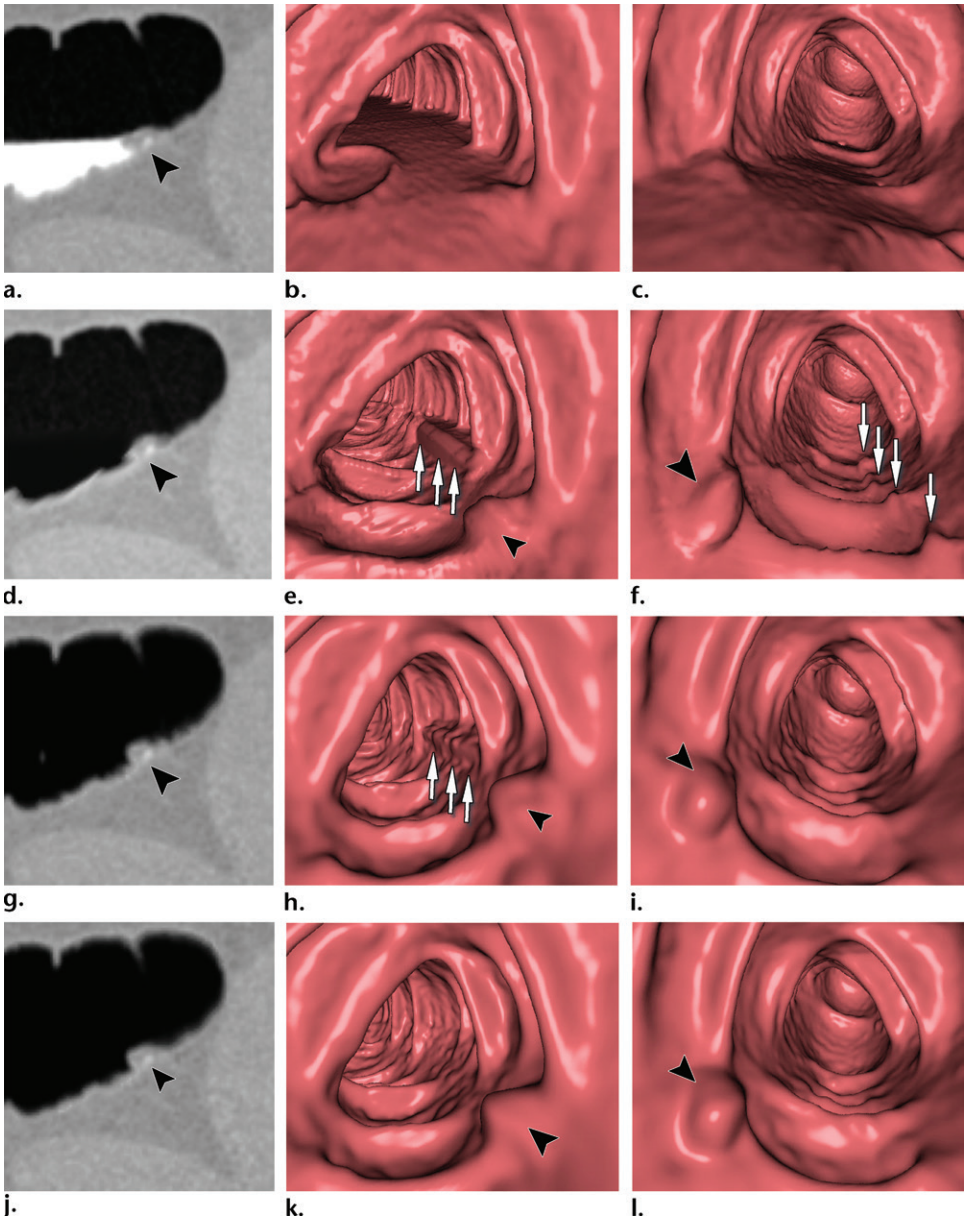

Figure 12. Electronic cleansing of tagged fluid with a partially submerged 10-mm polyp located at a three-material junction of soft tissue, tagged fluid, and air (arrowhead in all images except **b** and **c**). **(a–c)** Uncleansed sagittal CT colonographic image **(a)** clearly shows the polyp (arrowhead), but it is not as visible in the virtual endoluminal forward **(b)** and backward **(c)** views. **(d–f)** After cleansing with a conventional EC method, sagittal CT colonographic image **(d)** and virtual endoluminal views **(e, f)** show a distorted polyp with Type III artifacts (white arrows in **e** and **f**). **(g–i)** After cleansing with deep learning single-energy EC, the sagittal CT colonographic image **(g)** and virtual endoluminal views **(h, i)** show that the shape of the polyp is preserved; however, some Type III artifacts remain (white arrows in **h**) and imitate polyps, thereby distracting and misleading readers. **(j–l)** After cleansing with deep learning dual-energy EC, the sagittal CT colonographic image **(j)** and virtual endoluminal images **(k, l)** show that the shape and size of the polyp are preserved without generation of cleansing artifacts.

Another limitation of deep learning EC is that it remains challenging to determine what exactly a DCNN has learned. An extensive evaluation is needed to determine how the DCNN performs with new, unseen cases. If the DCNN does not perform as it should, it is not necessarily clear whether one should increase the number of training samples, increase the heterogeneity of training samples, or perhaps change the DCNN architecture in some way.

Conclusion

Conventional rigorous cathartic bowel cleansing for colorectal examinations can be reduced or avoided at CT colonography when patients orally ingest a contrast agent that mixes with

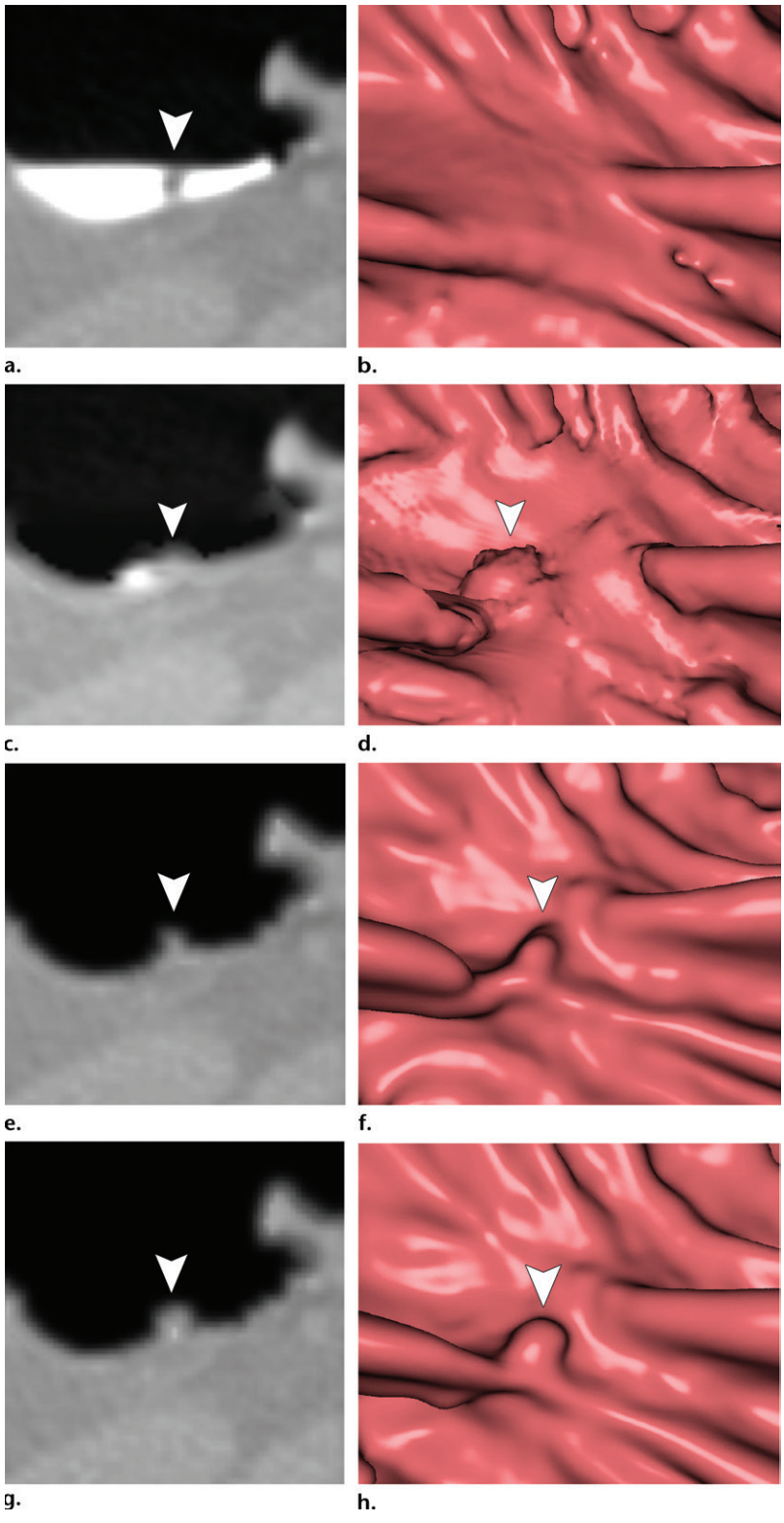

Figure 13. Electronic cleansing of semisolid tagged feces with a submerged 6-mm polyp. **(a)** The uncleansed axial CT colonographic image shows the polyp (arrowhead). **(b)** The virtual endoluminal view shows how the semisolid feces obstruct the view of the polyp. **(c, d)** After cleansing with a conventional EC method, the axial CT colonographic image **(c)** and virtual endoluminal view **(d)** show the distorted shape of the polyp (arrowhead). **(e, f)** After cleansing with the deep learning single-energy EC scheme, the axial CT colonographic image **(e)** and virtual endoluminal view **(f)** reveal the polyp (arrowhead), but the polyp appears inaccurately smaller. **(g, h)** After cleansing with the deep learning dual-energy EC scheme, axial CT colonographic image **(g)** and virtual endoluminal view **(h)** show that the size of the polyp (arrowhead) is preserved without producing cleansing artifacts.

residual fecal material and an EC method is used to remove tagged fecal material from the CT colonographic images and volumetric images. However, conventional EC methods tend to produce three types of cleansing artifacts: air-tagging boundaries (Type I), three-material boundaries (Type II), and three-material mixtures (Type III). Deep learning can be used to improve the quality of cleansing over that of conventional EC methods, especially in low-radiation-dose CT colonographic examinations in patients who have undergone noncathartic bowel preparation. Dual-energy CT can be used to optimize the quality of images cleansed with deep learning EC. Together,

deep learning and dual-energy CT colonography are promising approaches for providing a next-generation EC scheme that is a substantial improvement on the quality of EC of the colon at CT colonography.

***Disclosures of Conflicts of Interest.*—R.T.** *Activities related to the present article:* disclosed no relevant relationships. *Activities not related to the present article:* employment on the faculty of the Department of Information Science and Technology at the Institute of National Colleges of Technology, Oshima College, Japan. *Other activities:* disclosed no relevant relationships. **J.J.N.** *Activities related to the present article:* disclosed no relevant relationships. *Activities not related to the present article:* royalties from patents from the University of Chicago, licensed to Hologic and Median Technologies. *Other activities:* disclosed no relevant relationships. **D.R.** *Activities related to the present article:* disclosed no relevant relationships. *Activities not related to the present article:* support for travel to scientific meetings from Bracco and Bayer, honorarium for lectures from GE Medical Systems. *Other activities:* disclosed no relevant relationships. **H.Y.** *Activities related to the present article:* disclosed no relevant relationships. *Activities not related to the present article:* consultancy with Kentucky Imaging Technologies, royalties from patents from the University of Chicago, licensed to Hologic and Median Technologies. *Other activities:* disclosed no relevant relationships.

References

1. American Cancer Society. Cancer facts & figures 2018. Atlanta, Ga: American Cancer Society, 2018.
2. Levin B, Lieberman DA, McFarland B, et al. Screening and surveillance for the early detection of colorectal cancer and adenomatous polyps, 2008: a joint guideline from the American Cancer Society, the US Multi-Society Task Force on Colorectal Cancer, and the American College of Radiology. Gastroenterology 2008;134(5):1570–1595.
3. US Preventive Services Task Force, Bibbins-Domingo K, Grossman DC, et al. Screening for colorectal cancer: US Preventive Services Task Force recommendation statement. JAMA 2016;315(23):2564–2575.
4. Rockey DC, Paulson E, Niedzwiecki D, et al. Analysis of air contrast barium enema, computed tomographic colonography, and colonoscopy: prospective comparison. Lancet 2005;365(9456):305–311.
5. Pickhardt PJ. CT colonography for population screening: ready for prime time? Dig Dis Sci 2015;60(3):647–659.
6. Iannaccone R, Laghi A, Catalano C, et al. Computed tomographic colonography without cathartic preparation for the detection of colorectal polyps. Gastroenterology 2004;127(5):1300–1311.
7. Jensch S, Bipat S, Peringa J, et al. CT colonography with limited bowel preparation: prospective assessment of patient experience and preference in comparison to optical colonoscopy with cathartic bowel preparation. Eur Radiol 2010;20(1):146–156.
8. Lefere P, Gryspeerdt S, Baekelandt M, Van Holsbeeck B. Laxative-free CT colonography. AJR Am J Roentgenol 2004;183(4):945–948.
9. Zalis ME, Blake MA, Cai W, et al. Diagnostic accuracy of laxative-free computed tomographic colonography for detection of adenomatous polyps in asymptomatic adults: a prospective evaluation. Ann Intern Med 2012;156(10):692–702.
10. Neri E, Lefere P, Gryspeerdt S, Bemi P, Mantarro A, Bartolozzi C. Bowel preparation for CT colonography. Eur J Radiol 2013;82(8):1137–1143.
11. Pickhardt PJ, Choi JH. Electronic cleansing and stool tagging in CT colonography: advantages and pitfalls with primary three-dimensional evaluation. AJR Am J Roentgenol 2003;181(3):799–805.
12. Zalis ME, Perumpillichira J, Hahn PF. Digital subtraction bowel cleansing for CT colonography using morphological and linear filtration methods. IEEE Trans Med Imaging 2004;23(11):1335–1343.
13. Lu L, Jian B, Dijia D, Wolf M. A new algorithm of electronic cleansing for weak faecal-tagging CT colonography. In:Wu G, Zhang D, Shen D, Yan P, Suzuki K, Wang F (eds). International workshop on machine learning in medical imaging 2013: lecture notes in computer science; 8184:57–65.
14. Cai W, Zalis ME, Näppi J, Harris GJ, Yoshida H. Structure-analysis method for electronic cleansing in cathartic and noncathartic CT colonography. Med Phys 2008;35(7):3259–3277.
15. Serlie IW, Vos FM, Truyen R, Post FH, Stoker J, van Vliet LJ. Electronic cleansing for computed tomography (CT) colonography using a scale-invariant three-material model. IEEE Trans Biomed Eng 2010;57(6):1306–1317.
16. Eliahou R, Azraq Y, Carmi R, Mahgerefteh SY, Sosna J. Dual-energy based spectral electronic cleansing in non-cathartic computed tomography colonography: an emerging novel technique. Semin Ultrasound CT MR 2010;31(4):309–314.
17. Cai W, Lee JG, Zhang D, Kim SH, Zalis M, Yoshida H. Electronic cleansing in fecal-tagging dual-energy CT colonography based on material decomposition and virtual colon tagging. IEEE Trans Biomed Eng 2015;62(2):754–765.
18. Alvarez RE, Macovski A. Energy-selective reconstructions in x-ray computerized tomography. Phys Med Biol 1976;21(5):733–744.
19. Millner MR, McDavid WD, Waggener RG, Dennis MJ, Payne WH, Sank VJ. Extraction of information from CT scans at different energies. Med Phys 1979;6(1):70–71.
20. Johnson TR, Krauss B, Sedlmair M, et al. Material differentiation by dual energy CT: initial experience. Eur Radiol 2007;17(6):1510–1517.
21. LeCun Y, Bengio Y, Hinton G. Deep learning. Nature 2015;521(7553):436–444.
22. Gulshan V, Peng L, Coram M, et al. Development and validation of a deep learning algorithm for detection of diabetic retinopathy in retinal fundus photographs. JAMA 2016;316(22):2402–2410.
23. Esteva A, Kuprel B, Novoa RA, et al. Dermatologist-level classification of skin cancer with deep neural networks. Nature 2017;542(7639):115–118.
24. Sharma K, Rupprecht C, Caroli A, et al. Automatic segmentation of kidneys using deep learning for total kidney volume quantification in autosomal dominant polycystic kidney disease. Sci Rep 2017;7(1):2049.
25. Shen D, Wu G, Suk HI. Deep learning in medical image analysis. Annu Rev Biomed Eng 2017;19(1):221–248.
26. Jones N. Computer science:the learning machines. Nature 2014;505(7482):146–148.
27. Cai W, Yoshida H, Zalis ME, Näppi JJ, Harris GJ. Informatics in radiology: electronic cleansing for noncathartic CT colonography—a structure-analysis scheme. RadioGraphics 2010;30(3):585–602.
28. Yu L, Leng S, McCollough CH. Dual-energy CT-based monochromatic imaging. AJR Am J Roentgenol 2012;199(5 suppl):S9–S15.
29. Patino M, Prochowski A, Agrawal MD, et al. Material separation using dual-energy CT: current and emerging applications. RadioGraphics 2016;36(4):1087–1105.
30. Li JH, Du YM, Huang HM. Accuracy of dual-energy computed tomography for the quantification of iodine in a soft tissue-mimicking phantom. J Appl Clin Med Phys 2015;16(5):418–426.
31. Fulwadhva UP, Wortman JR, Sodickson AD. Use of dual-energy CT and iodine maps in evaluation of bowel disease. RadioGraphics 2016;36(2):393–406.
32. Chartrand G, Cheng PM, Vorontsov E, et al. Deep learning: a primer for radiologists. RadioGraphics 2017;37(7):2113–2131.
33. Pratt LY. Discriminability-based transfer between neural networks. Adv Neural Inf Process Syst 1993;5:204–211.
34. Oquab M, Bottou L, Laptev I, Sivic J. Learning and transferring mid-level image representations using convolutional neural networks. IEEE Conference on Computer Vision and Pattern Recognition, 2014; 1717–1724.
35. Girshick R, Donahue J, Darrell T, Malik J. Region-based convolutional networks for accurate object detection and segmentation. IEEE Trans Pattern Anal Mach Intell 2016;38(1):142–158.

36. Pontil M, Verri A. Support vector machines for 3D object recognition. IEEE Trans Pattern Anal Mach Intell 1998;20(6):637–646.
37. Cortes C, Vapnik V. Support-vector networks. Mach Learn 1995;20(3):273–297.
38. Tachibana R, Näppi JJ, Hironaka T, Kim SH, Yoshida H. Deep learning for electronic cleansing in dual-energy CT colonography. In: Tourassi GD, Armato SG, eds. Proceedings of SPIE: medical imaging 2016—computer-aided diagnosis. Vol 9785. Bellingham, Wash: International Society for Optics and Photonics, 2016; 97851M.
39. Tachibana R, Näppi JJ, Hironaka T, Kim SH, Yoshida H. Deep multi-spectral ensemble learning for electronic cleansing in dual-energy CT colonography. In: Armato SG, Petrick NA, eds. Proceedings of SPIE: medical imaging 2017—computer-aided diagnosis. Vol 10134. Bellingham, Wash: International Society for Optics and Photonics, 2017; 101340E.
40. Garcia-Garcia A, Orts-Escolano S, Oprea SO, Villena-Martinez V, Garcia-Rodriguez J. A review on deep learning techniques applied to semantic segmentation. arXiv 2017:1704.06857. https://arxiv.org/abs/1704.06857. Accessed October 5, 2018.
41. Krizhevsky A, Sutskever I, Hinton GE. ImageNet classification with deep convolutional neural networks. In: Proceedings of the 25th international conference on neural information processing systems. Periera F, Burges CJC, Bottou L, Weinberger KQ (eds). Lake Tahoe, Nev, December 3–6, 2012. Red Hook, NY: Curran Associates, 2012; 1097–1105.
42. BVLC Reference CaffeNet. https://github.com/BVLC/caffe/tree/master/models/bvlc_reference_caffenet. Accessed October 5, 2018.
43. Yushkevich PA, Piven J, Hazlett HC, et al. User-guided 3D active contour segmentation of anatomical structures: significantly improved efficiency and reliability. Neuroimage 2006;31(3):1116–1128.
44. Ota J, Tachibana R, Näppi JJ, Hironaka T, Regge D, Yoshida H. Performance evaluation of machine-learning-based electronic cleansing schemes for ultra-low-dose dual-energy CT colonography [abstr]. In: Radiological Society of North America scientific assembly and annual meeting program. Oak Brook, Ill: Radiological Society of North America, 2016; 148.
45. Näppi JJ, Hironaka T, Regge D, Yoshida H. Deep transfer learning for virtual endoluminal views for the detection of polyps in CT colonography. In: Tourassi GD, Armato SG, eds. Proceedings of SPIE: medical imaging 2016—computer-aided diagnosis. Vol 9785. Bellingham, Wash: International Society for Optics and Photonics, 2016; 97852B.
46. Näppi J, Yoshida H. Adaptive correction of the pseudo-enhancement of CT attenuation for fecal-tagging CT colonography. Med Image Anal 2008;12(4):413–426.